# Investigation of Microhole Quality of Nickel-Based Single Crystal Superalloy (CMSX-4) Processed by Ultrashort Laser

Dileep Madapana[1], Srinivasa Rao Nandam[2], and Deepak Marla[*1]
*Mechanical Engineering Department, Indian Institute of Technology Bombay, Mumbai, 400076 India*
*[2]Defence Metallurgical Research Laboratory, DRDO, Hyderabad, 500058, India*
*[*]Corresponding author's e-mail:dmarla@iitb.ac.in*

In the present study, ultrashort laser drilling of CMSX-4 alloy, a nickel-based single-crystal superalloy, was investigated to optimise hole quality by employing two scanning strategies (concentric circles and cross-hatch patterns) and a two-step processing methodology (concentric circle at the edges). The study systematically varied laser power and scanning speed while evaluating key parameters such as hole circularity, taper angle, surface roughness, and structural integrity. Results demonstrated that the concentric circles pattern combined with a two-step drilling approach yielded superior hole quality, achieving entry and exit circularities of 99.8% and 99.6%, respectively, with minimal taper angles (0.81° -1.52 °). In contrast, the cross-hatch pattern exhibited slightly higher taper angles (1.62°–2.11%). Single-step drilling resulted in significantly higher taper (up to 6.5°) and lower circularity. Surface roughness remained below 0.50 μm with two-step drilling, a substantial improvement over the conventional method. Cross-sectional micrographs revealed defect-free holes with minimal recast layers, no heat-affected zones, or micro-cracks. The two-step drilling methodology, incorporating an initial drilling phase followed by refinement with axial feed modulation, proved critical in enhancing hole geometry, dimensional accuracy, and surface finish. These findings highlight the potential of advanced scanning strategies and multi-step approaches for high-precision femtosecond laser drilling of single-crystal superalloys.
DOI: 10.2961/jlmn.2026.02.2003
**Keywords:** laser drilling, micro hole, CMSX-4, ultrashort laser, two-step drilling

## 1. Introduction

Nickel-based single-crystal superalloys, such as CMSX-4, are the material of choice for high-pressure turbine blades in aerospace and power generation systems due to their unparalleled high-temperature mechanical strength, creep resistance, and oxidation stability [1,2]. The absence of grain boundaries in these directionally solidified alloys eliminates weak points, enabling sustained performance under thermal and mechanical loads exceeding 90% of their melting point (~1300°C) [3]. A larger number of holes with a diameter of ≥ 500 μm is increasingly demanded in components such as combustor liners, fuel injector nozzles, and structural cooling systems, where enhanced airflow or coolant delivery is critical for thermal management under extreme operational loads [4–7]. For instance, modern cooling liners employ 1 mm holes to optimise fuel-air mixing and reduce emissions, requiring precise geometry control to maintain combustion efficiency [8]. Conventional mechanical drilling and electrical discharge machining (EDM) struggle to meet these demands, often inducing microcracks, recast layers, and heat-affected zones (HAZ) that degrade fatigue life [9,10]. Chen et al. [11] reported that the drilling of Ni-based superalloy using EDM-generated surfaces exhibited recast layers up to 20 μm thick, compromising oxidation resistance and leading to reduced fatigue performance. Akhtar et al. [12] reported that mechanical drilling of Ni-based superalloy led to rapid tool wear and subsurface plasticity due to the alloy's high work-hardening rate.

Laser drilling has emerged as a promising alternative, offering non-contact processing, high reproducibility, high aspect ratios, and flexibility in hole geometry [13,14]. However, challenges, including increased susceptibility to taper, recast layer accumulation, and thermal stress gradients, particularly in Ni-based superalloys, are still present [15,16]. Morar et al. [17,18] demonstrated that nanosecond (ns) pulsed lasers could drill CMSX-4 with reduced tool wear compared to mechanical methods, but thermal diffusion during longer pulses (~$10^{-9}$ s) caused recast layers (more than 20 μm) and microcracking along dendrite boundaries leads to significant reduction of fatigue life of the material. Similarly, Leigh et al. [19] observed oxidation of the recast layer formation and the presence of the HAZ of ns-laser-drilled CMSX-4, attributed to prolonged thermal exposure. Marimuthu et al. [20] have studied the characteristics of microhole formation during fibre laser drilling of Nimonic 263 nickel superalloy and reported that there is significant material redeposition and a heat-affected zone. These limitations have increased interest in ultrafast lasers, particularly femtosecond (fs) lasers (pulse duration ~$10^{-15}$ s), where material ablation occurs via non-thermal mechanisms, minimizing thermal damage [21, 22]. Recent advancements in femtosecond (fs) laser drilling have predominantly focused on polycrystalline superalloys such as Inconel 718, Inconel 792, and K24 [23–25]. Zhang et al. [25] successfully achieved taper-free holes with minimal defects in Inconel 792 by employing a nested circular scanning (inside-out) approach combined

with a two-step drilling strategy. Their use of a Yb-doped solid-state laser with a 400 fs pulse duration resulted in enhanced hole quality, primarily attributed to the mitigation of plasma shielding effects. Rujia et al. [26] demonstrated that a step drilling approach with a femtosecond laser has improved the micro-hole quality of thermal barrier-coated Inconel 718 alloy. In another study, Zhang et al. [23] optimised drilling methodologies for producing high-aspect-ratio holes in Inconel 718, utilising a Ti: sapphire laser with a pulse width of 50 fs. In this study, they have explored the effect of different drilling strategies on Inconel 718 plates to achieve high aspect ratio holes and reported that efficient laser drilling would be achieved by modifying the incident laser beam scattering and reflection with the hole walls. In contrast, the drilling of single-crystal superalloys such as CMSX-4 and DD6 presents significant challenges due to their anisotropic thermal and mechanical properties, which contribute to defect formation and process instability. As a result, achieving defect-free fs-laser-drilled holes in these materials remains highly complex. While some studies have investigated fs-laser drilling in DD6, a Ni-based single-crystal superalloy [27–30], research on CMSX-4 remains largely unexplored. Li et al.[29] reported that femtosecond laser drilling of DD6 alloys exhibits a size effect, influencing geometry, efficiency, and hole wall quality. As scanning diameter increases, taper rises, efficiency increases, then declines, and walls transition from defective to nano-striped, governed by spot overlap rate and energy shielding effects. Du et al. [27] optimised femtosecond laser drilling parameters for DD6 single-crystal alloy using an orthogonal test and genetic algorithm, analysing six factors on micro-hole quality. Li et al. [28] demonstrated the femtosecond laser drilling of DD6 alloy using the two-step helical drilling processing to avoid recast layers, microcracks, and microvoid formation due to laser energy shielding and heat accumulation during the single-step processing. Currently, the available literature on CMSX-4 is limited to studies employing nanosecond laser drilling, with no significant reports on femtosecond laser drilling for this alloy. Critical gaps persist in understanding how fs-laser parameters (e.g., pulse energy, scanning speed, and scanning strategy) interact with Ni-based single-crystal superalloys to influence hole quality. First, while parameter optimisation has been explored for polycrystalline alloys [23–25], the role of scanning strategies (concentric circles vs. cross-hatch pattern) in managing thermal gradients and resolidification dynamics in single-crystal systems remains unaddressed. Second, the impact of multi-step drilling methodologies—such as combining initial ablation with axial feed modulation for geometry refinement—on hole circularity, taper angle, and surface roughness has not been systematically investigated. This study addresses these challenges by systematically investigating femtosecond laser drilling of CMSX-4, with a focus on the interplay between scanning strategies (concentric circles vs. cross-hatch pattern), multi-step drilling methodologies, and hole quality. In this study, the quality of the drill has been quantified in terms of heat-affected zones, recast layers, hole circularity, taper angle, and surface roughness to showcase how ultrashort pulse processing, combined with optimized strategies, mitigates thermal defects in single-crystal systems.

## 2. Materials and Methods

The work material used in the present study, a Ni-based alloy (CMSX-4 alloy) with the following composition by weight: Co (9.6%), Cr (6.5%), Ta (6.5%), W (6.4%), Al (5.6%), Re (3.0%), Ti (1.0%), Mo (0.6%), and Hf (0.1%), with the balance is Ni. The material was prepared in the form of samples with dimensions of 40 mm × 15 mm × 1.24 mm. Prior to laser drilling, all samples were cleaned for 10 minutes using an ultrasonic cleaning to remove contaminants and avoid their impact on the drilling process. The micro-machining system included a Yb solid-state femtosecond laser system equipped with a Galvo scanner and an XYZ positioning system. The femtosecond laser (Farros, Light Conversion) had a pulse width of 206 fs, a maximum average output power of 10 W, a wavelength of 1035 nm, and a repetition rate of 200 kHz. The optical setup consisted of a beam expander, a Galvo scanning system (Scanworld), and several mirrors, as shown in Fig. 1. All experiments were conducted in a Class 1000 clean room under controlled conditions of 22 °C temperature and 45% relative humidity.

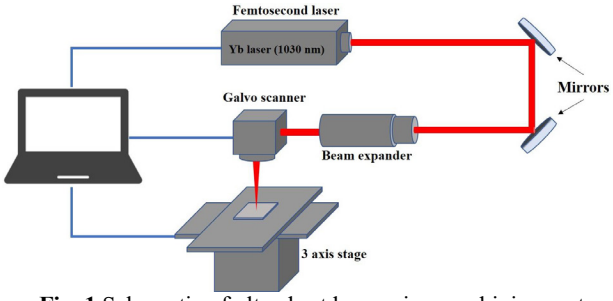


**Fig. 1** Schematic of ultrashort laser micromachining system used for laser drilling of CMSX-4 alloy.

Holes with a diameter of 500 µm were processed during the experiments. The laser beam was focused on the CMSX-4 surface using an F-theta lens with a focal length of 100 mm, resulting in a focal spot diameter of approximately 40 µm and a depth of focus of about 0.1 mm. The drilling was performed in ambient air without the use of a shielding gas. After laser drilling, the samples were cleaned with alcohol and dried for further analysis. Experiments were conducted using two scanning patterns: concentric circles with 50% overlap and circles (processing from innermost to outermost) with cross-hatch pattern filling with 75% overlap. The feed rate was maintained at a constant 0.5 mm/min, while laser power (5 W and 7 W) and scan speed (100, 200, and 300 mm/s) were varied. In a two-step drilling strategy, concentric circles with a thickness of 150 µm processed towards the outside with a feed rate of 0.5 mm/min were employed to improve the circularity of the drilled holes. The laser powers of 5 W and 7 W were selected to represent the minimum power required for stable through-hole formation and a higher power enabling enhanced ablation efficiency without excessive plasma shielding, respectively. Different scan overlap ratios were employed to suit the scanning strategies: a higher overlap (70%) was used for the cross-hatch pattern to ensure continuous material removal at scan intersections, while a lower overlap (50%) was sufficient for the concentric circle strategy due to its inherent rotational symmetry and uniform pulse distribution. A detailed schematic of the drilling strategies used is presented in Fig. 2. The two-step

drilling strategy adopted in this study involves sequential processing of the same drilled holes, rather than independent drilling steps, as illustrated in Fig. 2. In the first step, through-holes are fabricated in a single-step manner by scanning the laser over the entire hole area using either concentric circle or cross-hatch scanning strategies. This primary step is responsible for bulk material removal and hole breakthrough; however, it may introduce taper, redeposited material, and edge irregularities due to plasma shielding, beam scattering, and energy attenuation along the hole depth.

In the second step, the same holes produced in the first step are reprocessed using concentric circle scanning confined to a narrow peripheral region (~150 μm from the hole edge), while maintaining the same axial feed rate. This secondary step acts purely as a refinement process rather than a fresh drilling operation. It selectively removes redeposited material formed during the first step, homogenizes energy deposition along the hole sidewalls, and corrects geometrical deviations, thereby significantly improving exit circularity, reducing taper angle, and enhancing edge quality without appreciable additional bulk material removal.

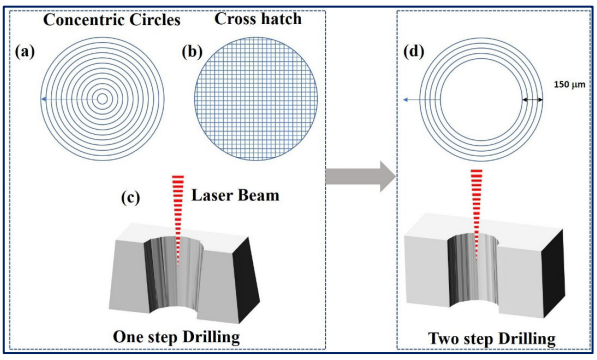


**Fig. 2** Schematic of scanning strategies used during ultrashort laser drilling of CMSX-4 (a) concentric circles, (b) circle with cross-hatch, (c) schematic of the cross section in one step, and (d) scanning strategy and schematic in the secondary step drilling.

Post-laser drilling, the hole quality was evaluated based on parameters such as heat-affected zone (HAZ), resolidified material, hole circularity (HC), taper angle (TA), and surface roughness inside the holes. Hole geometry was studied using a 3D non-contact optical profilometer (Zeta-20, Zeta Instruments), while microstructure and composition were analysed using a dual vacuum high-resolution field emission scanning electron microscope (FESEM, JSM IT510, JEOL).
Hole circularity (HC) has been measured using Eq. 1:

$$HC = \frac{D_{min}}{D_{max}} \times 100\% \, . \qquad (1)$$

$HC$ = 100% shows the fully circular, and $D_{min}$ and $D_{max}$ show the minimum and maximum hole diameters in the hole.
The taper angle (TA) has been calculated using Eq.2.

$$TA = tan^{-1} \frac{D_i - D_o}{2T} \, , \qquad (2)$$

where $TA$ denotes the taper angle, T is the sample thickness, and $D_i$ and $D_o$ are the diameters of the entry and exit, respectively.

## 3. Results and Discussion

Figure 3 shows the optical micrographs of holes drilled on CMSX-4 alloy using a femtosecond laser under two scanning strategies: cross-hatch (c.f Fig. 3a–d and a′–d′) and concentric circles (c.f Fig. 3e–h and e′–h′). Fig. 3 clearly illustrates the influence of laser parameters and scan strategy on both entry and exit morphology. At 5 W with a cross-hatch pattern (Figs. 3a–d), the entry are circular with well-defined edges. As scanning speed increases from 100 mm/s to 200 mm/s, a slight decrease in hole diameter is observed from 496.6 μm to 488.2 μm, suggesting lower energy deposition per unit area due to reduced interaction time. However, despite identical laser power and scanning speed, noticeable differences are observed between Fig. 3a and Fig. 3c, as well as between Fig. 3b and Fig. 3d. These differences arise from the directional nature of the cross-hatch scanning strategy, where orthogonal scan patterns produce non-uniform pulse overlap and localized energy accumulation at scan intersections. This results in uneven ablation fronts and asymmetric material removal. The exit geometries (c.f Figs. 3a′–d′) are relatively smaller and slightly elliptical, indicating a taper in the drilled holes. The ellipticity of the exit hole may be due to polarisation-dependent energy absorption on the hole wall, and beam reflection, causing uneven energy distribution, distorting the laser path, and leading to asymmetrical material removal [31–33]. At the higher laser power of 7 W (c.f. Figs. 3e-h and e'-h'), both scanning strategies produce relatively larger and more uniform holes at the entry and exit compared to those obtained at 5 W. The increase in laser power enhances ablation efficiency and penetration depth, thereby reducing energy attenuation along the hole depth. Under identical scanning speeds (e.g., Fig. 3e vs Fig. 3g), the concentric circle scanning strategy results in improved entry–exit symmetry compared to the cross-hatch strategy. This improvement is attributed to the rotationally symmetric pulse overlap inherent to concentric circle scanning, which promotes more uniform energy homogenization along the hole perimeter and depth. Consequently, the exits in Fig. 3 (e′–h′) appear more circular and wider than those obtained using the concentric circles pattern at the same power. Increasing the laser power to 7 W significantly influences the circularity of the hole. For both scanning patterns, the entry diameters (c.f Figs. 3e–h) become slightly larger at 7 W laser power. The exits (c.f Figs. 3e′–h′) also become wider and more circular with reduced ovality compared to 5 W, indicating that higher laser power partially compensates for energy losses and beam distortion within the hole, leading to improved circularity and ablation stability.

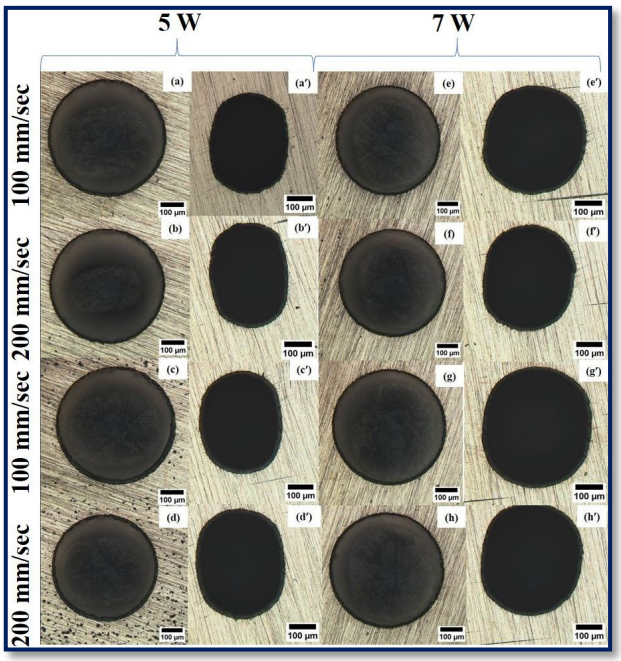


**Fig. 3** Optical micrographs of the drill images under varied laser processing conditions, one-step laser drilling with cross-hatch pattern (a-d) entry (a′-d′) exit and concentric circles pattern (e-h) entry, (e′-h′) exit.

Figure 4 presents the circularity values of holes using one-step concentric circles and cross-hatch with circular scanning strategies. The circularity was calculated from optical micrographs (c.f Fig. 3) using the ratio of the minor axis to the major axis of the hole profile, with unity indicating a perfect circle. The analysis offers insight into the geometric precession of the holes and the effect of the scanning strategy on morphological changes. At a laser power of 5 W and a scanning speed of 100 mm/s, the entry circularity in the cross-hatch pattern is 0.97. In contrast, the exit side exhibited a significantly lower circularity of 0.78, indicating notable tapering and asymmetric material removal through the hole depth. This loss of circularity at the exit may be attributed to energy attenuation along the depth. The ellipticity observed here is consistent with prior reported literature in ultrafast drilling of Ni-based alloys, where insufficient lateral energy distribution resulted in asymmetric ablation fronts [25]. Conversely, the concentric circles pattern strategy under the same conditions resulted in entry and exit circularities of 0.99 and 0.89, respectively. The improvement is attributed to enhanced pulse overlap and distribution of energy uniformity, which promotes symmetrical ablation through increased pulse superposition and reduced local energy accumulation [34]. As a result, the concentric circles pattern mitigates taper formation and produces more circular and uniform holes.

When the scanning speed was increased to 200 mm/s at 5 W, the circularity in the cross-hatch pattern decreased further, with the exit dropping to 0.72, while the concentric circles strategy retained better shape integrity, with exit circularity remaining above 0.85. The decrease in circularity at higher scan speeds may be attributed to reduced laser–material interaction time, leading to incomplete material removal at the trailing edge of the beam path. An increase in laser power to 7 W positively influenced circularity across both scan patterns due to the higher peak fluence (~5.6 J/cm²). For the cross-hatch pattern, the exit circularity improved to 0.82 at 100 mm/s and 0.80 at 200 mm/s, indicating deeper and more uniform drilling but still falling short of ideal values. In contrast, concentric circles scanning at 7 W resulted in exit circularity values of 0.90 at 100 mm/s and 0.88 at 200 mm/s, with improved geometries.

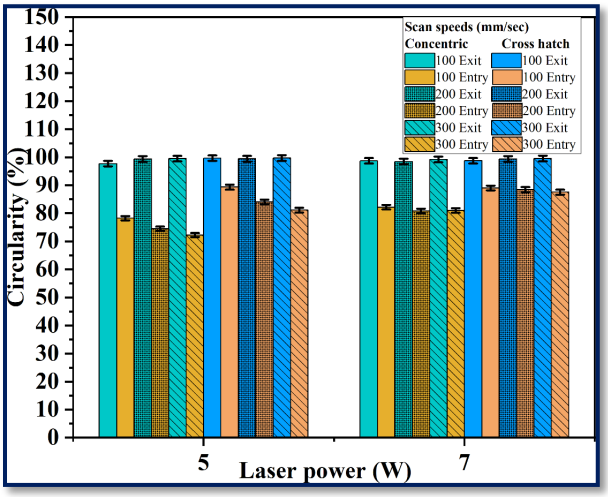


**Fig. 4** A bar chart showing the circularity of the ultrafast laser drill with one-step drilling of concentric circles and cross-hatch pattern.

Figure 5 shows the variation in taper angle for microholes fabricated using one-step ultrafast laser drilling with concentric circles and cross-hatch with circular scanning strategy under varied laser powers and scanning speeds. The taper angle was calculated based on the difference between entry and exit diameters measured from optical micrographs (c.f Fig. 3). At a laser power of 5 W and scanning speed of 100 mm/s, the taper angle in the cross-hatch pattern reached a maximum of 5.5°, whereas the concentric circles scanning configuration resulted a significantly lower taper of 3.4°. The reduced taper angle shows the superior energy homogenization achieved through uniform energy distribution during concentric circle scanning, which facilitates more uniform ablation throughout the hole depth. In contrast, the cross-hatch scanning tends to favour energy localisation at the entry due to inefficient material removal, leading to a wider opening and reduced penetration at the exit, thereby increasing the taper. As the scanning speed was increased to 200 mm/s, taper angles increased for both strategies due to reduced effective pulse overlap and energy deposition. In the cross-hatch pattern, the taper increased to 6.2°, while the concentric circle still had a relatively lower angle of 4.6°. At a higher power of 7 W, taper angles showed improvement overall, reflecting enhanced ablation efficiency and deeper penetration due to increased peak fluence. For instance, at 100 mm/s, the taper in the cross-hatch scan decreased to 5.1°, while in the concentric circles, it further reduced to 3.5°. Even at 200 mm/s, the taper angle remained relatively low at 3.8° in the concentric circle's strategy, compared to 5.3° in the cross-hatch pattern. These results demonstrate that higher laser power can partially compensate for the reduced

interaction time at higher speeds, but the scan strategy still plays a dominant role in controlling hole geometry.

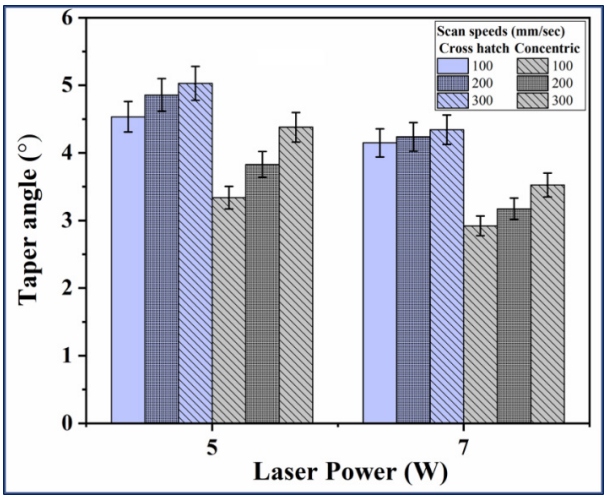


**Fig. 5** A bar chart showing the taper angle of the ultrafast laser drill with one-step drilling of concentric circles and cross-hatch pattern.

Figure 6 presents cross-sectional SEM micrographs of the edge morphology of femtosecond laser-drilled through-holes in a Ni-based single-crystal superalloy under different process parameters. The effect of the scanning strategy (concentric circles vs. cross-hatch pattern) and laser power on the hole edge quality is examined. In one-step drilling (c.f Figs. 6a–d), significant variations in edge integrity are observed between the two scanning strategies. At a laser power of 5 W and a scan speed of 100 mm/s, the concentric circle scanning strategy (c.f Fig. 6a) results in a relatively uneven edge profile, indicating incomplete material removal. In contrast, the cross-hatch pattern at the same power (c.f. Fig. 6c) shows more effective bulk material removal; however, the hole edges display pronounced micro-notches and surface irregularities, highlighted in the annotated regions. This may be attributed to enhanced energy accumulation in the cross-hatch pattern, leading to preferential material removal. Although the cross-hatch pattern in single-step processing facilitates efficient material removal with improved circularity and lower taper angles, the edge finish is inferior to that of the concentric circle pattern. At a higher laser power of 7 W (c.f Figs. 6b and 6d), both scanning strategies show improved material removal. However, to achieve a fully straight hole with enhanced edge quality, secondary processing is required.

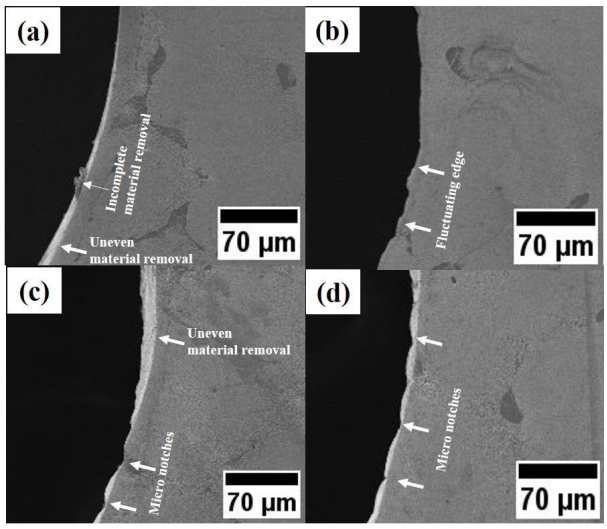


**Fig. 6** Edges of the laser-drilled Ni-based single crystal superalloy at (a,c) 5 W 100 mm/sec, (b,d) 7 W 100 mm/sec. Where (a,b) concentric circles (c,d) cross-hatch pattern in one-step processing.

Figure 7 displays optical micrographs of through-holes fabricated in CMSX-4 superalloy via two-step femtosecond laser drilling, employing different laser powers and scan strategies. The entry (a–d) and exits (a′–d′) correspond to cross-hatch and concentric circle scanning patterns processed at 5 W (a, c) and 7 W (b, d), with a constant scan speed of 100 mm/s. At 5 W, the cross-hatch pattern (Fig. 7a, a′) produced relatively symmetric entry but exhibited irregular exit edges, indicative of insufficient energy delivery at greater depths.

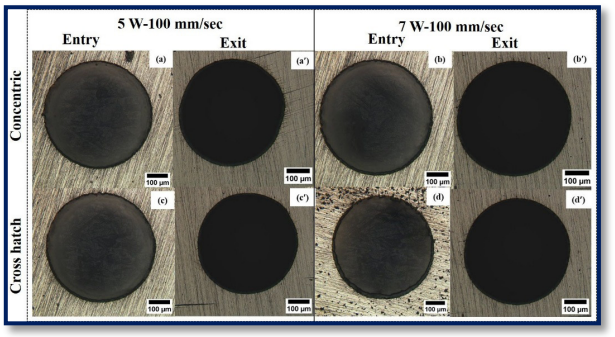


**Fig. 7** Optical images of the ultrafast laser drilled two step processing, (a,b) are with cross hatch and (c,d) with concentric circles, processed with (a,c) at 5 W and 100 mm/sec and (b,d) 7 W and 100 mm/sec where (a-d) are the entry and (a′-d′) are the exits of the drilling.

Conversely, the concentric circle strategy (Fig. 7c, c′) at the same power level improved exit morphology, suggesting enhanced fluence uniformity; however, complete material removal was not achieved. Increasing the laser power to 7 W resulted in notable enhancements for both scanning patterns. Both concentric circles and cross-hatch (Fig. 7b, b′ and Fig. 7d, d′) demonstrated improved entry and exit geometries with reduced taper, attributable to increased ablation efficiency. The holes produced are uniform, circular, and burr-free profiles at both entry and exit, underscoring the advantages of increased power and the two-step drilling process. These findings indicate that both concentric and cross-hatch scanning approach at 7 W delivers optimal hole quality,

characterised by minimal taper and superior edge finish, in ultrafast laser drilling of CMSX-4 superalloy.

Figure 8 compares the circularity values of through-holes drilled using ultrafast laser pulses under one-step and two-step drilling methodologies. Under one-step drilling, the maximum circularity of the exit was observed to be approximately 0.90, whereas it improved significantly to 0.99 in the two-step approach. This enhanced circularity of ~9.1% indicates that two-step drilling leads to more symmetric and well-defined hole geometries. The improved circularity can be attributed to reduced debris accumulation due to the presence of a pre-shaped cavity in the first step. This facilitates a more cylindrical hole shape and contributes to higher circularity values in the two-step drilling process. When combined with two-step drilling, a better-quality hole is achieved in the second step, with a better circularity even at the exit side, which is generally prone to irregularities due to re-deposition in single-step processing. These results are in line with previous studies, such as that by Zhang et al. [25], which demonstrated that multi-pass femtosecond drilling with optimised scan strategies significantly improves exit hole circularity and overall dimensional fidelity in nickel-based superalloys.

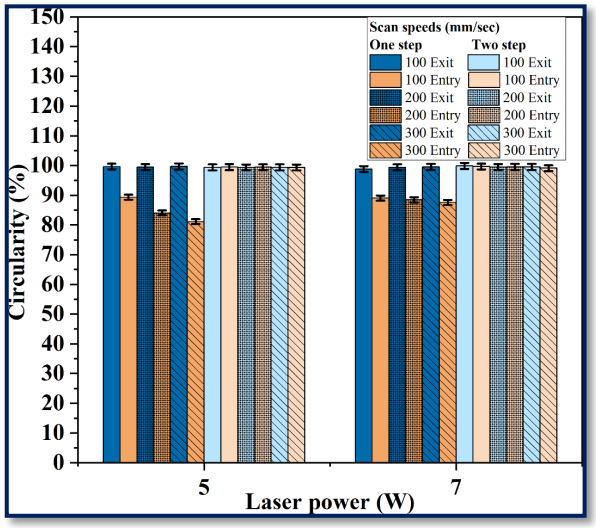


**Fig. 8** A bar chart showing the circularity of the ultrafast laser drill with one-step and two-step drilling of concentric circle strategy.

Figure 9 shows the variation in taper angle for ultrafast laser-drilled through-holes performed using concentric circle scanning under two different methods: one-step and two-step drilling. In the one-step drilling, the minimum taper angle was measured to be approximately in the range of 2.91°, while it significantly reduced to 0.81° in the two-step processing. This reduced taper angle to ~72% demonstrates the effectiveness of two-step drilling in improving directional ablation and material removal. In the past, Li et al. [28] and Zhang et al. [25] have demonstrated that multi-pass drilling improves the aspect ratio and straightness of holes in nickel-based superalloys, findings consistent with those of this study.

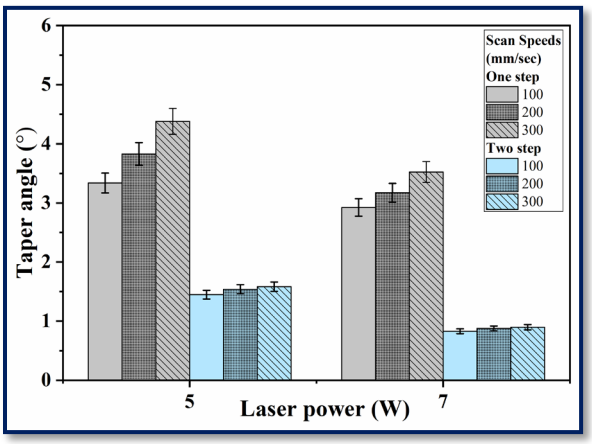


**Fig. 9** A bar chart showing the taper angle of the ultrafast laser drill with one-step and two-step drilling of concentric circle pattern.

Two-step drilling (c.f Figs. 10a–d) significantly enhances edge morphology compared to one-step processing. For the concentric circles pattern at 7 W and 100 mm/s (c.f Fig. 10a), the hole edge appears smooth and continuous, with a nearly straight profile and minimal local waviness. This indicates effective removal of residual irregularities introduced during the primary drilling step. The corresponding circular pattern hole after concentric circle refinement (c.f Fig. 10c) also exhibits a smooth edge with a noticeable reduction in micro-notches and edge fluctuations previously observed in one-step drilling (c.f. Fig. 6). The absence of pronounced edge irregularities under these conditions demonstrates effectiveness of the secondary refinement step in redistributing laser energy more uniformly along the hole perimeter and promoting efficient debris evacuation.

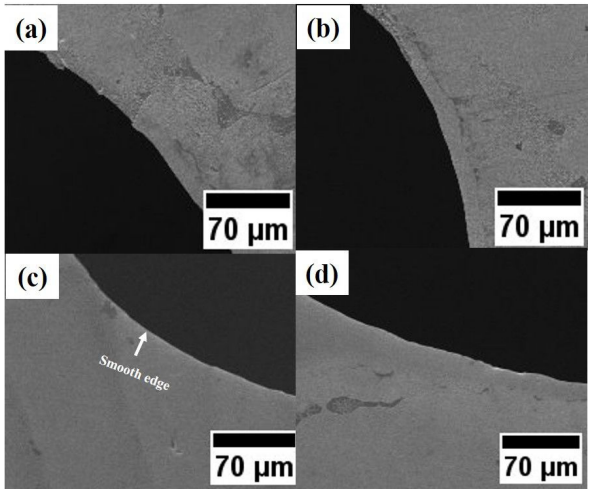


**Fig. 10** Edges of the laser-drilled Ni-based single crystal superalloy at (a,c) 5 W 100 mm/sec, (b,d) 7 W 100 mm/sec. Where (a,b) cross-hatch (c,d) concentric circles pattern in two-step processing.

Figure 11 presents high-resolution SEM high-magnification images showing the recast layer formation at the periphery of femtosecond laser-drilled through-holes in a Ni-based single crystal superalloy under varying scanning strategies and processing conditions. The recast layer, formed due to the rapid resolidification of vaporised and ejected material, exhibits distinct morphological characteristics based on the

interplay of laser power, scan pattern, and energy deposition strategy. For one-step drilling (c.f Figs. 11a and 11b), a dense, network-like recast layer is observed along the hole periphery. In the concentric circles scanning approach (c.f Fig. 11a), the recast layer appears uniformly distributed with microcracking. The cross-hatch pattern (c.f Fig. 11b), in contrast, exhibits a more irregular recast layer with discontinuities and porous structures, likely arising from repeated overlap of scan vectors, leading to non-uniform ablation front propagation and uncontrolled melt expulsion. During two-step drilling (c.f Figs. 11c and 11d), a uniform recast layer without any defects is evident in both scanning strategies. There is a marginal change in the recast layer thickness observed for one-step drilling, 0.3 µm to 0.27 µm in two-step drilling. This can be attributed to the secondary material removal approach in two-step drilling, which facilitates better heat dissipation and prevents beam distortion. These observations highlight the significance of scanning strategy and two-step processing in preventing the formation of a recast layer during femtosecond laser drilling.

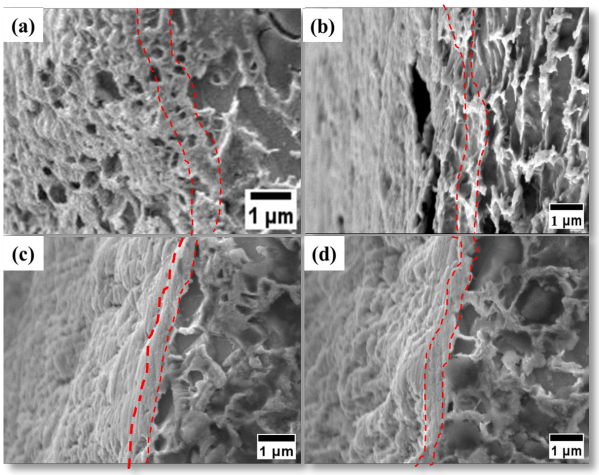


**Fig. 11** Recast layer formation of the laser-drilled Ni-based single crystal superalloy at 7 W 100 mm/sec (a,c) concentric circles, (b,d) cross-hatch pattern and (a,b) at one step and (c,d) at two-step drilling.

Figure 12 presents a comparative analysis of the cross-sectional surface topography and roughness of femtosecond laser-drilled Ni-based superalloy samples under different processing conditions. The three-dimensional surface profiles in Figs. 12(a) and 12(b) correspond to single-step and two-step drilling strategies, respectively, both employing a concentric circle scanning pattern at a laser power of 7 W and a scan speed of 100 mm/s. Fig. 12(c) shows the average surface roughness ($S_a$) for different processing parameters. In the single-step process (c.f Fig. 12a), a pronounced surface irregularity is evident, with significant height variations extending up to ~30 µm. This roughness arises due to non-uniform melt ejection and the presence of recast material, which undergoes rapid solidification due to the ultrafast nature of the laser-material interaction. The uneven heat distribution in the single-step process results in localised thermal gradients, leading to microstructural inhomogeneities and surface asperities. In contrast, the two-step process (c.f Fig. 12b) exhibits a more uniform topography with reduced peak-to-valley height variations, indicating improved surface quality. The second step likely facilitates the removal of residual recast material and promotes a more uniform ablation front, thereby minimising defect formation. The enhanced surface smoothness can be attributed to the redistribution of energy over multiple laser passes, allowing for better melt ejection dynamics.

Figure 12(c) further corroborates these observations by presenting the $S_a$ values for both scanning strategies at two different laser powers (5 W and 7 W). The results indicate that single-step processing consistently results in higher surface roughness compared to two-step processing. Additionally, irrespective of the drilling approach, the cross-hatch scanning strategy exhibits lower $S_a$ values compared to the concentric circle strategy due to uniform energy distribution and enhanced material removal. Notably, at 7 W, the two-step approach significantly reduces $S_a$, demonstrating the efficacy of multi-step processing in mitigating surface irregularities.

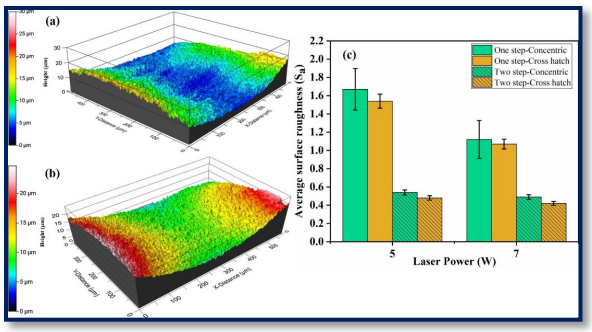


**Fig. 12** 3D profile of the cross-section and roughness profiles of 7W 100 mm/sec with a cross-hatch in (a) one-step processing, (b) two-step processing, and (c) bar chart of the roughness under various processing conditions.

## 4. Conclusions

In this study, the influence of scanning strategy and processing parameters on the microstructural integrity and surface quality of ultrashort laser-drilled holes in a Ni-based single-crystal superalloy (CMSX-4) was systematically investigated. A comparative analysis was conducted between concentric circles and cross-hatch scan patterns, implemented through both single-step and two-step drilling approaches. The key findings are summarised as follows:

1)Optical and scanning electron micrographs demonstrated that the concentric circles pattern significantly enhances hole quality compared to cross-hatch.

2)The concentric circle pattern combined with a two-step methodology achieved superior hole quality, with entry and exit circularities of 99.8% and 99.6%, respectively. Two-step laser drilling achieved a ~72% improvement in the reduction of taper angle over one-step processing.

3)Edge morphology analysis revealed that while the cross-hatch pattern improves circularity and reduces taper, it can lead to uneven edge profiles in one-step processing. A secondary refinement step using the concentric circle pattern enhances edge quality and ensures a fully straight hole.

4)Cross-sectional topography analysis indicates that the two-step drilling process substantially reduces surface roughness ($S_a$) by promoting uniform ablation and efficient melt ejection. The cross-hatch scanning strategy provides a

more uniform fluence distribution, leading to smoother surface profiles.

5)The two-step approach minimised recast layer defects and produced near-taper-free holes due to reduced plasma confinement and beam scattering effects.

6)The optimised two-step process not only improved dimensional accuracy but also contributed to better laser energy distribution, reducing thermal accumulation and mitigating potential surface damage.

**Acknowledgement**

The authors would like to acknowledge DMRL, Hyderabad, for providing the material. The authors would also acknowledge the Dual Vacuum HR SEM Facility (Dept. of MEMS), Zeta Microscope (MTL Lab, Dept. of ME), and IIT Bombay for their support.

**References**

[1] R. C. Reed: "Single-Crystal Superalloys for Blade Applications", in The Superalloys: Fundamentals and Applications (Cambridge University Press, Cambridge, 2006) p.121.

[2] S. R. Nandam, A. V. Rao, A. A. Gokhale, and S. S. Joshi: J. Mater. Eng. Perform., 33, (2024) 7054.

[3] A. Nowotnik: Ref. Modul. Mater. Sci. Mater. Eng., 1, (2016) 1.

[4] L. Pang, N. Zhao, H. Xu, Z. Li, H. Zheng, and R. Yang: Appl. Therm. Eng., 234, (2023) 121308.

[5] Z. Li, and Y. Dai: Mater., 15, (2022) 1973.

[6] C. Lu, E. Song, C. Xu, Z. Ni, X. Yang, and Q. Dong: J. Mar. Sci. Eng., 11, (2023) 596.

[7] Y. Q. Cheng, W. L. Li, C. Jiang, G. Wang, W. Xu, and Q. Y. Peng: Meas. Sci. Technol., 33, (2021) 015018.

[8] Z. P. Xu, H. R. Zhu, C. L. Liu, and X. L. Li: Phys. Fluids, 35, (2023) 105150.

[9] A. Behera, A. K. Sahoo, and S. S. Mahapatra: Adv. Mater. Process. Technol., 11, (2024) 1085.

[10] P. S. Gowthaman, and S. Jeyakumar: Mater. Today Proc., 18, (2019) 4782.

[11] Z. Chen, J. Moverare, R. L. Peng, and S. Johansson: Procedia CIRP, 45, (2016) 307.

[12] W. Akhtar, J. Sun, P. Sun, W. Chen, and Z. Saleem: Front. Mech. Eng., 9, (2014) 106.

[13] C. Y. Yeo, S. C. Tam, S. Jana, and M. W. S. Lau: J. Mater. Process. Technol., 42, (1994) 15.

[14] W. Schulz, U. Eppelt, and R. Poprawe: J. Laser Appl., 25, (2013) 012006.

[15] C. A. McNally, J. Folkes, and I. R. Pashby: Mater. Sci. Technol., 20, (2004) 805.

[16] Z. Y. Li, X. T. Wei, Y. B. Guo, and M. P. Sealy: Mach. Sci. Technol., 19, (2015) 361.

[17] N. I. Morar, R. Roy, J. Mehnen, S. Marithumu, S. Gray, T. Roberts, and J. Nicholls: Int. J. Adv. Manuf. Technol., 95, (2018) 4059.

[18] N. I. Morar, S. Gray, J. Nicholls, and J. Mehnen: Procedia Manuf., 16, (2018) 67.

[19] S. Leigh, K. Sezer, L. Li, C. Grafton-Reed, and M. Cuttell: Proc. Inst. Mech. Eng. Part B J. Eng. Manuf., 224, (2010) 1005.

[20] S. Marimuthu, M. Antar, and J. Dunleavey: Precis. Eng., 55, (2019) 339.

[21] K. C. Phillips, H. H. Gandhi, E. Mazur, and S. K. Sundaram: Adv. Opt. Photonics, 7, (2015) 684.

[22] Y. Jia and F. Chen: APL Photonics, 8, (2023) 090901.

[23] N. Zhang, M. Wang, M. Ban, L. Guo, and W. Liu: J. Mater. Res. Technol., 28, (2024) 1415.

[24] Q. Li, L. Yang, C. Hou, O. Adeyemi, C. Chen, and Y. Wang: Opt. Lasers Eng., 114, (2019) 22.

[25] F. Zhang, J. Wang, X. Wang, J. Zhang, Y. Hayasaki, D. Kim, and S. Sun: Opt. Laser Technol., 143, (2021) 107335.

[26] R. Wang, X. Dong, K. Wang, X. Sun, Z. Fan, and W. Duan: Opt. Lasers Eng., 121, (2019) 406.

[27] T. Du, X. Liang, Y. Yu, L. Zhou, Z. Cai, L. Wang, W. Jia, and X. Pan: Met., 13, (2023) 333.

[28] M. Li, Z. Wen, P. Wang, Y. Liu, Z. Li, and Z. Yue: J. Mater. Process. Technol., 312, (2023) 117827.

[29] M. Li, Z. Wen, P. Wang, Z. Li, G. Lu, Y. Liu, and Z. Yue: J. Manuf. Process., 116, (2024) 77.

[30] D. Zhang, Z. Song, Z. Luo, X. Guo, and Z. Wen: Coatings, 14, (2024) 137.

[31] Z. A, G. Zou, H. Yu, B. Feng, C. Du, and L. Liu: Precis. Eng., 86, (2024) 153.

[32] A. Zhanwen, G. Zou, W. Zhao, B. Feng, C. Du, Y. Wu, Y. Xiao, J. Huo, Y. Wu, and L. Liu: Appl. Phys. A Mater. Sci. Process., 129, (2023) 1.

[33] Z. Zhang, Z. Xu, C. Wang, S. Liu, Z. Yang, Q. Zhang, and W. Xu: Opt. Laser Technol., 139, (2021) 106968.

[34] T. E. Lizotte and O. Ohar: Proc. SPIE, Vol. 8130, (2011) 81300G.

(Received: August 22, 2025, Accepted: March 1, 2026)